



Cite this: DOI: 10.1039/c6nr05516h

Received 13th July 2016,  
Accepted 1st September 2016

DOI: 10.1039/c6nr05516h

www.rsc.org/nanoscale

## Complex surface structure of (110) terminated strontium titanate nanododecahedra†

Lawrence A. Crosby,<sup>a</sup> Robert M. Kennedy,<sup>b</sup> Bor-Rong Chen,<sup>a</sup> Jianguo Wen,<sup>c</sup> Kenneth R. Poeppelmeier,<sup>b</sup> Michael J. Bedzyk<sup>a</sup> and Laurence D. Marks<sup>\*a</sup>

The surface structure of (110) faceted strontium titanate nanoparticles synthesized *via* solvothermal method has been resolved using high-resolution electron microscopy (HREM). We demonstrate that the surface is a titania-rich structure containing tetrahedrally coordinated TiO<sub>4</sub> units similar to the family of (*n* × 1) reconstructions observed on (110) surfaces of bulk crystalline strontium titanate. When compared with prior results for (001) terminated strontium titanate single crystals made with traditional transmission electron microscopy (TEM) sample preparation techniques, the results demonstrate that many models for oxide nanoparticles need to be revisited. This work serves as a reminder that attention must be paid to the surface of nanoparticles. Even with a simple perovskite as the starting point the end result can be very complex. As more materials are synthesized on the nanoscale, this will become increasingly important to take into consideration.

### Introduction

A variety of applications including catalysis,<sup>1–5</sup> electronic devices,<sup>6,7</sup> and energy<sup>8–10</sup> have motivated significant attention in the area of oxide materials. This is true of both mesoscale oxides with flat surfaces and nanoscale oxide particles. A wide range of techniques have been used to make these materials. One of the most popular is the solvo/hydrothermal method primarily because of its versatility.<sup>11</sup> Many different compounds can be synthesized, the reactions are scalable, and the size and shape of the particles can be controlled through the choice of precursors, solvents, and concentration. For the specific case of strontium titanate, many shapes and sizes of crystallites have been synthesized, ranging from nanowires,<sup>12</sup>

spheres,<sup>13</sup> to cubes<sup>14</sup> and dodecahedra.<sup>15</sup> In general, these syntheses involve precursors for the metallic A and B sites as well as a capping agent such as acetic acid<sup>16</sup> or oleic acid.<sup>17,18</sup>

In most of the nanoparticle literature, it has been assumed that surfaces are simple truncations of the bulk material with, in some cases, chemisorbed ligands. The reality may be more complicated. Work in surface science on single crystals has discovered the existence of surface reconstructions, which are atomic arrangements distinctly different from the underlying substrate. These arrangements result from the instability induced by changes in the bonding and coordination at the surfaces. This is well-known<sup>19</sup> and some of the most famous cases have been observed in the semiconductor silicon,<sup>20</sup> as well as metals silver and gold.<sup>21,22</sup> For the specific case of oxides, these can be well described by classical bonding analyses such as the bond valence sum (BVS) approach (see ref. 23 for a recent detailed discussion).

Is this relevant for oxide nanoparticles? Are they small versions of mesoscale crystals with similar surfaces, or do they contain different structures? If so, at what size are there differences? For applications this certainly matters. In the case of catalysis, oxide supports are known to play a crucial role in reactivity through a variety of physical phenomena. These include the metal-support interaction,<sup>24</sup> the coordination environment of the atomic species adsorbed on the metal<sup>25</sup> and the degree of dispersion of the metallic species.<sup>26</sup> One such support, (001) faceted strontium titanate nanocrystals (nanocuboids), serves as an important illustration. Both the chemistry and structure of the surface depend upon the synthesis method,<sup>27</sup> with one case resulting in a reconstructed surface. These different surfaces in turn lead to different epitaxies of platinum deposited by atomic layer deposition onto these materials and different catalytic behavior.<sup>28,29</sup> Another example in the recent literature<sup>30</sup> is the (001) surface of TiO<sub>2</sub> nanorods, which reconstructs in a manner similar to that observed on bulk surfaces.

In addition to catalysis, the surface structure will influence many other properties such as corrosion resistance of the

<sup>a</sup>Department of Materials Science and Engineering, Northwestern University, Evanston, IL 60208, USA

<sup>b</sup>Department of Chemistry, Northwestern University, Evanston, IL 60208, USA

<sup>c</sup>Center for Nanoscale Materials, Argonne National Laboratory, Lemont, IL 60439, USA

†Electronic supplementary information (ESI) available. See DOI: 10.1039/c6nr05516h

oxide, localization of electrons and holes at the surface in response to light, and interactions with biological molecules and cells to name just a few.

Beyond applications, there are also some fundamental scientific issues. For appropriate (ideally six sigma) control of the shape, we need to understand what is taking place during growth of the nanoparticles, the details beyond just a recipe to produce them. As reviewed recently,<sup>31</sup> while the core models that explain nanoparticle shape, thermodynamics and kinetics are well understood many details are not. Surfactants in the fluid phase are known to have significant effects, but whether this is because of thermodynamics of adsorption on different structures or kinetics is not well understood.

In this work, we report on the surface structure of (110) faceted strontium titanate nanocrystals. We observed the presence of a complex surface structure corresponding to the  $(n \times 1)$  reconstructions<sup>28,32</sup> previously observed on mesoscale surfaces. We demonstrate that the atomic structure of nanoparticles needs to be considered as a surface science problem and that they are not simple terminations of the bulk as the majority of the existing literature has assumed.

## Experimental

Strontium titanate (STO) rhombic dodecahedra were synthesized following a method published by Dong *et al.*,<sup>15</sup> which was modified by the authors. The primary modifications are the use of titanium tetrabutoxide ( $\text{Ti}(\text{OBu})_4$ ) instead of titanium tetrachloride ( $\text{TiCl}_4$ ) as titanium precursor, the use of strontium acetate ( $\text{Sr}(\text{Ac})_2$ ) instead of  $\text{SrCl}_2$ , and the use of sodium hydroxide ( $\text{NaOH}$ ) instead of lithium hydroxide ( $\text{LiOH}$ ). Additionally, the solution was not chilled in an ice bath. With these changes, the details of the synthesis are as follows:

Solution A was prepared by dissolving 2.9 mL acetic acid into 37.1 mL deionized water, then adding 1.9 g  $\text{Sr}(\text{Ac})_2$  while stirring. Solution B was prepared by adding 3.1 mL  $\text{Ti}(\text{OBu})_4$  into 31.5 g of glycerol while stirring for at least 5 minutes. Solution A was then added into solution B while stirring for at least 2 minutes. Then 10 mL of 10 M  $\text{NaOH}$  was added dropwise while stirring. The resulting mixture (translucent yellow-white) was placed into a Teflon-lined autoclave for 36–48 hours of solvothermal treatment at a temperature of 240 °C, with ramping rate of 1 °C  $\text{min}^{-1}$  for the heating.

The resulting white powder was washed by dispersing in water and centrifuging repeatedly until the pH was neutral (7) as measured by pH strips, then dried in an oven at 80 °C overnight. TEM samples were prepared by suspending a few milligrams of powder in approximately 10 mL of ethanol and sonicating for 15 minutes. The dispersed nanoparticles were then drop-cast with a pipet onto lacey carbon TEM grids. The samples were characterized with several microscopes including a Hitachi HD2300 equipped with a secondary electron detector, a probe-corrected JEOL ARM 200CF, and the Argonne chromatic aberration-corrected TEM (ACAT, a FEI Titan 80-300 ST

with a  $C_s/C_c$  image corrector) at Argonne National Laboratory. X-ray diffraction (XRD) samples were prepared by compacting several grams of the powder sample into a pellet on a low-background glass slide. In order to identify the phase purity of the synthesized sample, the survey scattering profile was completed with an Ultima X-ray diffractometer (Rigaku), with a  $\text{Cu K}\alpha$  source operating at 40 kV. To minimize the instrument peak width when calculating the crystallite size, an ATXG X-ray diffractometer (Rigaku) equipped with Ge (111) monochromator was utilized. The composition of the STO dodecahedra was analyzed with X-ray photoemission spectroscopy (XPS) (Thermo Scientific ESCALAB 250Xi) using a monochromatic  $\text{Al K}\alpha$  (1486.74 eV) X-ray source as well as Energy Dispersive Spectroscopy (EDS) on the Hitachi HD2300 using a Thermo Scientific dual-detector  $\text{Si}(\text{Li})$  EDS system. The detailed analysis appears in the ESI.†

The XRD spectra were fingerprinted using the MDI JADE X-ray crystallographic database. The MacTempasX software package (an implementation of the multislice method<sup>33</sup> and non-linear imaging theory) was employed to simulate the HREM images. The simulated imaging parameters were optimized to find the closest match to the real microscope conditions. This tuning was done using bulk motifs within the experimental dataset. The procedure for doing so is described in the ESI.†

## Results and discussion

The general morphology of the resulting nanoparticles was dodecahedral with predominantly (110) faceting as shown in a secondary electron microscopy (SEM) image in Fig. 1a. There was minor faceting present, as (001) is visible at high magnification (Fig. 2). The particles were phase pure as verified by XRD (ESI Fig. S1†) with an average domain size of 180 nm (ESI Fig. S2†), with minimal surface contamination evident in the XPS results (ESI Fig. S3†) and no evidence for any variations in composition based upon the EDS results (ESI Fig. S4†). While there were particles that exhibited sintering, the majority of the particles imaged exhibited sharp faceting with little, if any, corner rounding. Additionally, there was no evidence of dislocations, twins, or other defects in the TEM data. When imaged along the [001] direction with high angle annular dark-field (HAADF), the reduced contrast of the dodecahedra is consistent with thin areas at the corners as shown in Fig. 1b. This is visible in Fig. 2 which shows that the corners are atomically flat at the edges for two different nanoparticles.

Utilizing the tool of profile-view imaging,<sup>34</sup> we observed the surface structure of the nanoparticles along two zone axes. By comparing the observed experimental contrast with simulated images for both  $\text{SrTiO}$  and O terminated surface (the two possible nominal  $(1 \times 1)$  bulk truncations) it is clear that neither is a plausible structural match (see Fig. S7 and S8 in ESI†). The  $(3 \times 1)$  and  $(4 \times 1)$  reconstructions, whose structure is reported previously,<sup>28</sup> were used as the basis for additional simulations. These structures, previously observed on annealed bulk single

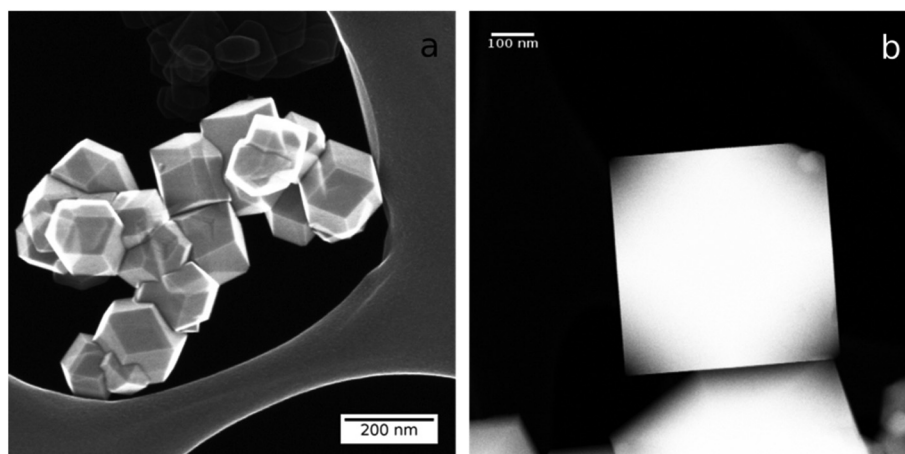


**Fig. 1** Low magnification SEM (a) and HAADF (b) images demonstrating dodecahedral shape of the nanoparticles. The three-dimensional character is evident in (a), and shows in (b) *via* the intensity changes.

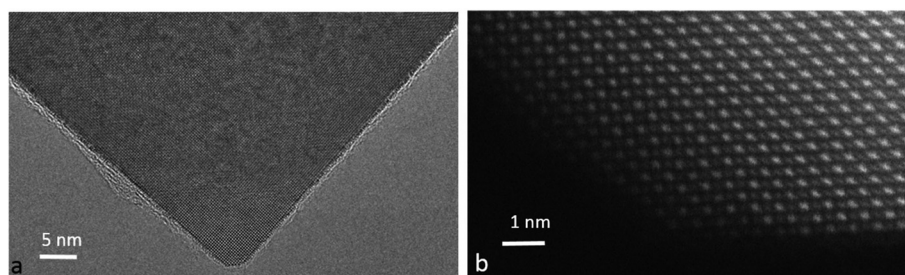


**Fig. 2** High-resolution (a) CTEM and (b) HAADF images from two different nanoparticles showing atomically sharp faceting.

crystal samples of (110) STO, were solved *via* direct methods analysis<sup>35</sup> of transmission electron diffraction data combined with refinement using density functional theory. The change in coordination environment from octahedral to tetrahedral for the titanium at the surface explains the stability of these reconstructions. The simulated contrast agrees well with the experimental results for both surface structures but we cannot rule out co-existence of the two.

When viewed along the [001] direction (see Fig. 3) there is an additional corrugation of the (110) surface along the  $[\bar{1}10]$  direction. As shown in the inset, this can be explained by either of the  $(3 \times 1)$  or  $(4 \times 1)$  reconstructions. Comparing the contrast between the simple  $(1 \times 1)$  truncations, one can see subtle differences. For instance, there is an additional small bright spot below the surface arrowed in Fig. 3 which is not present with a simple bulk termination. With respect to

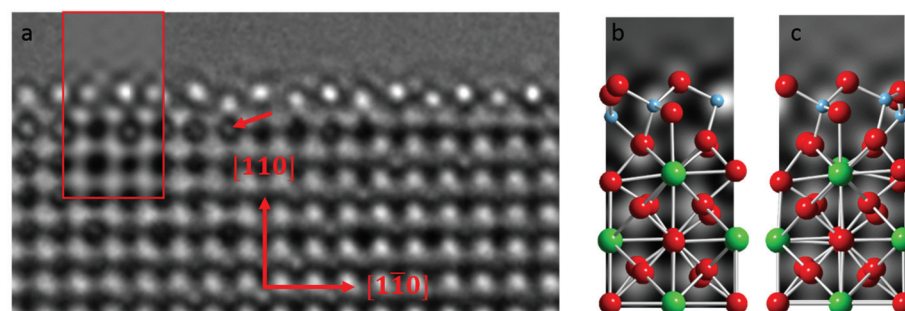


**Fig. 3** (a) Experimental profile image down the [001] zone, with an image simulation (red box) for a  $(3 \times 1)$  reconstruction inset. In (b) image simulations for the  $(3 \times 1)$  and (c)  $(4 \times 1)$  reconstructions are shown with the atomic structure superimposed. The  $(3 \times 1)$  gave the best fit to experiment for this area, although in other regions it was the  $(4 \times 1)$ .

quantitative agreement, the cross-correlation values were 0.79 for the  $(3 \times 1)$  and 0.77 for the  $(4 \times 1)$  along the  $[001]$  zone.

As a secondary check results for the  $[110]$  zone axis are shown in Fig. 4 which confirm the interpretation that the surface is likely a mixture of several  $(n \times 1)$  reconstructions with  $(3 \times 1)$  and  $(4 \times 1)$  yielding the best match. The best cross-correlation values for the  $(3 \times 1)$  and  $(4 \times 1)$  were 0.69 and 0.65 respectively. All imaging parameters appear in the accompanying ESI.†

The reconstructions observed are stable in vacuum for a surface  $\text{TiO}_2$  excess of about 1.5 per  $1 \times 1$  surface unit cell, and are relatively easy to reproduce for bulk  $(110)$  surfaces. The shape of a nanoparticle is controlled by a combination of factors involving both the nucleation of new steps as well as the relative energies and chemisorption characteristics of different surfaces. An overview of some of the terms as well as additional literature can be found in Marks & Peng.<sup>31</sup>

During solvothermal synthesis there is exchange between the surface of the oxide nanoparticles and the surrounding solute. In almost all cases this will be a local thermodynamic equilibrium process. At lower  $\text{p}K_a$  the  $(001)$  facets are growing fast, so vanish from the kinetic-growth shape; at higher  $\text{p}K_a$

the situation reverses and the  $(110)$  facets are growing out of existence. We note that the results of Dong *et al.*<sup>15</sup> indicate sharp corners and edges at high  $\text{p}K_a$ , indicators of kinetic control with a relatively large chemical potential difference between the solid and surrounding fluid.

Since we did not observe significant crystal defects for samples which contained quite large particles, this indicates that this is a case of conventional nucleation and growth. Other similar syntheses have been demonstrated to have growth affected by confinement of liquid crystal micro-emulsions<sup>18</sup> as well as shrinking and Ostwald ripening.<sup>36</sup> The corners and edges of the nanoparticles were sharp, which indicates that the chemical potential difference between the solid and the surrounding environment was relatively large<sup>37</sup> and that the overall growth was *via* a kinetic-Wulff construction route (see ref. 31 and references therein).

Glycerol served as either a co-solvent, surfactant, or both, altering the kinetics of growth and/or the thermodynamics of which surface is lowest energy. Since  $(110)$  facets are small for the Wulff shape in oxygen (see ref. 38 and references therein) the surfactant here has clearly had a significant effect. It is known that the synthesis conditions can stabilize different

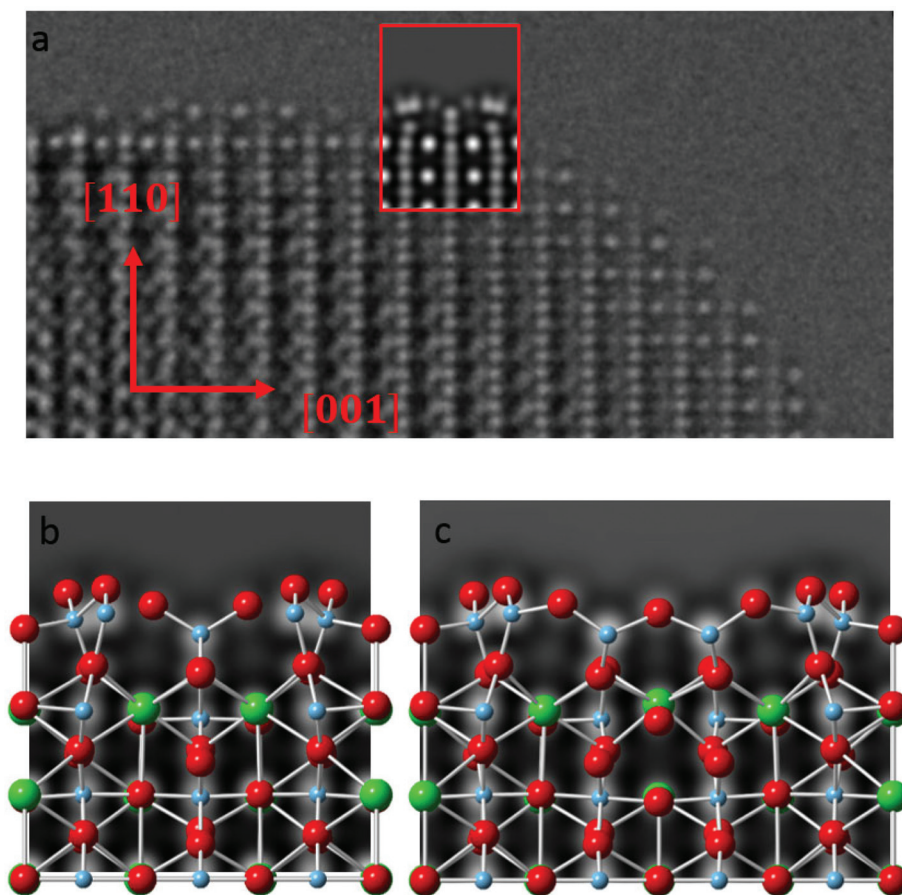


Fig. 4 (a) Experimental profile image down the  $[1\bar{1}0]$  zone, with an image simulation (red box) for a  $(4 \times 1)$  reconstruction inset. In (b) image simulations for the  $(3 \times 1)$  and (c)  $(4 \times 1)$  reconstructions are shown with the atomic structure superimposed. The  $(3 \times 1)$  gave the best fit to experiment for this area, although in other regions it was the  $(4 \times 1)$ .

crystallographic facets, and even different chemical environments for a given facet. The structure of a surface, both bulk and on nanoparticles, is determined by thermodynamics, kinetics, or a combination of the two. Surface chemisorbed species such as water or surfactants can have large effects, as is well known. In our case the reconstructions on the (110) surfaces are stabilized during the nanoparticle growth phase, and remain stable in air as the samples are stored at ambient conditions.

Dong *et al.*<sup>15</sup> experimentally establish a correlation between the faceting and the  $pK_a$  and concentration of the polyol added to the system, more (110) at lower  $pK_a$ , *i.e.* stronger acids. To understand this, they performed density functional theory calculations for chemisorption of water, methanol, and ethylene glycol on a simplified model of the surface. Our results indicate that unfortunately they chose an inappropriate model for the surface. The correct one is a titanium-rich structure with the tetrahedra of the  $(n \times 1)$  reconstructions.

## Conclusions

In summary, we have demonstrated that the (110) faceted STO nanoparticles synthesized *via* solvothermal method have complex surface structures, which matches results obtained on (001) faceted nanoparticles. The observed surface matches well with the known structures for the  $(3 \times 1)$  and  $(4 \times 1)$  reconstructions. This is noteworthy due to the different methods by which reconstructed surfaces were obtained: the bulk samples by mechanical polishing, ion beam thinning, and subsequent annealing at high temperatures; the results herein by wet chemical synthesis *via* solvothermal preparation of nanoparticles at comparatively moderate temperatures. While different methods will yield different kinetic routes to surface structures, the thermodynamics will always be important.

We conclude that surfaces of nanoparticles require the same considerations of thermodynamics and surface science as do mesoscale crystals.

## Acknowledgements

This material is based upon work supported by the U. S. Department of Energy, Office of Science, Office of Basic Energy Sciences under Award Number DOE DE-FG02-03-ER154757. LC also acknowledges support from a National Science Foundation Graduate Fellowship. Use of aberration-corrected TEM at the Center for Nanoscale Materials, an Office of Science user facility, supported by the U. S. Department of Energy, Office of Science, Office of Basic Energy Sciences, under Contract No. DE-AC02-06CH11357.

## References

- 1 C. N. Satterfield, *Heterogeneous Catalysis in Industrial Practice*, McGraw-Hill, New York, 2nd edn, 1996.
- 2 H. H. Kung and E. I. Ko, *Chem. Eng. J.*, 1996, **64**, 203–214.
- 3 G. Centi, F. Cavani and F. Trifiro, *Selective Oxidation by Heterogeneous Catalysis*, Kluwer Academic, New York, 1st edn, 2001.
- 4 C. H. Bartholomew and R. J. Farrauto, *Fundamentals of Industrial Catalytic Processes*, John Wiley & Sons, 2nd edn, 2005.
- 5 I. E. Wachs and T. Kim, in *Metal Oxide Catalysis*, Wiley-VCH Verlag GmbH & Co. KGaA, 2009, pp. 487–498.
- 6 M. E. Franke, T. J. Koplín and U. Simon, *Small*, 2006, **2**, 36–50.
- 7 M. Fernández-García and J. A. Rodríguez, in *Encyclopedia of Inorganic Chemistry*, John Wiley & Sons, Ltd, 2006.
- 8 W. J. E. Beek, M. M. Wienk and R. A. J. Janssen, *Adv. Mater.*, 2004, **16**, 1009–1012.
- 9 P. Simon and Y. Gogotsi, *Nat. Mater.*, 2008, **7**, 845–854.
- 10 E. Mitchell, F. De Souza, R. K. Gupta, P. K. Kahol, D. Kumar, L. Dong and B. K. Gupta, *Powder Technol.*, 2015, **272**, 295–299.
- 11 D. R. Modeshia and R. I. Walton, *Chem. Soc. Rev.*, 2010, **39**, 4303–4325.
- 12 U. A. Joshi and J. S. Lee, *Small*, 2005, **1**, 1172–1176.
- 13 Y. Wang, H. Xu, X. Wang, X. Zhang, H. Jia, L. Zhang and J. Qiu, *J. Phys. Chem. B*, 2006, **110**, 13835–13840.
- 14 K. Fujinami, K. Katagiri, J. Kamiya, T. Hamanaka and K. Koumoto, *Nanoscale*, 2010, **2**, 2080–2083.
- 15 L. Q. Dong, H. Shi, K. Cheng, Q. Wang, W. J. Weng and W. Q. Han, *Nano Res.*, 2014, **7**, 1311–1318.
- 16 F. A. Rabuffetti, H. S. Kim, J. A. Enterkin, Y. M. Wang, C. H. Lanier, L. D. Marks, K. R. Poeppelmeier and P. C. Stair, *Chem. Mater.*, 2008, **20**, 5628–5635.
- 17 C. Friderichs, N. Zotov and W. Mader, *Eur. J. Inorg. Chem.*, 2015, **2015**, 288–295.
- 18 L. H. Hu, C. D. Wang, S. Lee, R. E. Winans, L. D. Marks and K. R. Poeppelmeier, *Chem. Mater.*, 2013, **25**, 378–384.
- 19 G. A. Somorjai, *Principles of Surface Chemistry*, Prentice Hall, Englewood Cliffs, NJ, 1972.
- 20 D. J. Chadi, *Phys. Rev. Lett.*, 1979, **43**, 43–47.
- 21 P. W. Palmberg and T. N. Rhodin, *Phys. Rev.*, 1967, **161**, 586–588.
- 22 L. D. Marks and D. J. Smith, *Nature*, 1983, **303**, 316–317.
- 23 J. A. Enterkin, A. E. Becerra-Toledo, K. R. Poeppelmeier and L. D. Marks, *Surf. Sci.*, 2012, **606**, 344–355.
- 24 G. L. Haller and D. E. Resasco, *Adv. Catal.*, 1989, **36**, 173–235.
- 25 M. Che and C. O. Bennett, *Adv. Catal.*, 1989, **36**, 55–172.
- 26 G. C. Bond, *Chem. Soc. Rev.*, 1991, **20**, 441–475.
- 27 Y. Lin, J. Wen, L. Hu, R. M. Kennedy, P. C. Stair, K. R. Poeppelmeier and L. D. Marks, *Phys. Rev. Lett.*, 2013, **111**, 156101.
- 28 J. A. Enterkin, A. K. Subramanian, B. C. Russell, M. R. Castell, K. R. Poeppelmeier and L. D. Marks, *Nat. Mater.*, 2010, **9**, 245–248.
- 29 J. A. Enterkin, R. M. Kennedy, J. Lu, J. W. Elam, R. E. Cook, L. D. Marks, P. C. Stair, C. L. Marshall and K. R. Poeppelmeier, *Top. Catal.*, 2013, **56**, 1829–1834.

- 30 W. Yuan, Y. Wang, H. Li, H. Wu, Z. Zhang, A. Selloni and C. Sun, *Nano Lett.*, 2016, **16**, 132–137.
- 31 L. D. Marks and L. Peng, *J. Phys.: Condens. Matter*, 2016, **28**, 053001.
- 32 F. Li, Z. Wang, S. Meng, Y. Sun, J. Yang, Q. Guo and J. Guo, *Phys. Rev. Lett.*, 2011, **107**, 036103.
- 33 J. M. Cowley and A. F. Moodie, *Acta Crystallogr.*, 1957, **10**, 609–619.
- 34 L. D. Marks, *Phys. Rev. Lett.*, 1983, **51**, 1000–1002.
- 35 E. Landree, C. Collazo-Davila and L. D. Marks, *Acta Crystallogr., Sect. B: Struct. Sci.*, 1997, **53**, 916–922.
- 36 H. Q. Zhan, Z. G. Chen, J. L. Zhuang, X. F. Yang, Q. L. Wu, X. P. Jiang, C. L. Liang, M. M. Wu and J. Zou, *J. Phys. Chem. C*, 2015, **119**, 3530–3537.
- 37 D. Alpay, L. Peng and L. D. Marks, *J. Phys. Chem. C*, 2015, **119**, 21018–21023.
- 38 L. Crosby, J. Enterkin, F. Rabuffetti, K. Poeppelmeier and L. Marks, *Surf. Sci.*, 2015, **632**, L22–L25.